DEVELOPMENT OF AN ALTERNATIVE TO THE HELIUM-3 BASED ACTIVE WELL COINCIDENCE COUNTER WITH BORON COATED STRAWS

A Thesis

by

COSTNER MCLAINE QUICK

Submitted to the Office of Graduate and Professional Studies of
Texas A&M University
in partial fulfillment of the requirements for the degree of

MASTER OF SCIENCE

Chair of Committee,	Craig Marianno
Committee Members,	Marvin Adams
	Sunil Khatri
Head of Department,	Yassin Hassan

August 2018

Major Subject: Nuclear Engineering

ABSTRACT

An active well coincidence counter (AWCC) is used for Nondestructive Assay (NDA) of special nuclear material. This counter was developed for the International Atomic Energy Agency (IAEA) to perform in field inspections. Whether the sample that is analyzed spontaneously fissions or requires a neutron source to induce fission, multiple neutrons are emitted simultaneously in the event of fission. If the sample being quantified spontaneously fissions, then the AWCC can be used in passive mode. When the sample requires neutron induced fission, a small neutron source can be placed in equidistant compartments and the AWCC will be used in active neutron coincidence mode.

Coincident neutron characteristics vary depending on the isotope, which allows for the sample to be identified and quantified. Since the inception of the AWCC, the detector has utilized ^{3}He. The shortage of ^{3}He gas in the world has created a necessity for an alternative neutron detection medium. A promising neutron detection option is boron-coated straws (BCS). The efficacy of BCS as a neutron detector has been proven in radiation portal monitors, vehicle mounted modular detectors, and handheld detectors, but has yet to be assessed in an AWCC with its original footprint. Analysis of the original AWCC with ^{3}He and alternatives with ^{10}B-lined tubes and BCS was done in MCNPX. The comparison of the original technology to the proposed alternative was done in an effort to find a viable option for replacing ^{3}He as the detection medium.

ACKNOWLEDGEMENTS

There are many people whom deserve my gratitude for helping make this research possible. First, I must thank my research chair, Dr. Craig Marianno for all of his help and guidance after my original advisor departed from the University. I am also grateful to have had an opportunity to intern at the Pacific Northwest National Laboratory (PNNL) site. The assistance of Dr. Edward Siciliano, with whom I met with during my time at PNNL, was invaluable and made the analysis of the simulations in this thesis possible. I would also like to thank Dr. Sunil Khatri and Dr. Marvin Adams for taking the time to review my proposal and thesis and to agree to be on my committee.

CONTRIBUTORS AND FUNDING SOURCES

Contributors

This work was supervised by a thesis committee consisting of my advisor Professor Marianno and Professor Adams of the Department of Nuclear Engineering and Professor Khatri of the Department of Electrical & Computer Engineering.

All work for the thesis was completed by the student, in collaboration with Edward Siciliano of the Pacific Northwest National Laboratory.

Funding Sources

Graduate study was supported by a Graduate Teaching Assistantship from Texas A&M University.

NOMENCLATURE

AWCC	Active Well Coincidence Counter
^{10}B	Boron-10
BCS	Boron-Coated Straws
BF_3	Boron Trifluoride
^{252}Cf	Californium-252
cps	Counts per second
τ	Die-away time
eV	Electron volt
FOM	Figure-of-merit
^{3}He	Helium-3
HDPE	High Density Polyethylene
HEU	Highly Enriched Uranium
IAEA	International Atomic Energy Agency
LANL	Los Alamos National Laboratory
LEU	Low enriched uranium
MCNPX	Monte Carlo N-Particle (eXtended) code
mR/h	Milli-Roentgen per hour
ε	Neutron detection efficiency
NDA	Non-Destructive Assay
PNNL	Pacific Northwest National Laboratory
Pu	Plutonium
PH	Pulse height (F8) tally

PSD	Pulse shape discrimination
RPM	Radiation Portal Monitor
TCE	Total Count Efficiency
U	Uranium

TABLE OF CONTENTS

Page

LIST OF FIGURES

Page

LIST OF TABLES

Page

1. INTRODUCTION

1.1 Radiation Detection Basics

There are 92 naturally occurring elements and from these, there are 287 naturally occurring isotopes. About 15 of these naturally occurring isotopes are unstable (radioactive) while the 20 man-made elements make up over 1600 isotopes that are all radioactive. Each isotope of any given element fundamentally has the same chemical properties but vary physically depending upon their nuclear stability and atomic mass. This characteristic forces one to utilize physical techniques to separate isotopes or to alter an isotope's relative concentration [1].

Some unstable high mass number nuclides may undergo spontaneous fission. Spontaneous fission results in fission daughter products that have atomic numbers from 27 to 62 that have atomic mass numbers between 65 to 160, plus one to four neutrons, on average, per spontaneous fission. The high atomic mass number nuclides that do not undergo spontaneous fission at a significant rate (such as ^{235}U) may undergo fission when bombarded by free neutrons. The free neutron must have sufficiently high energy before impact with the heavy nuclide to induce fission [1].

The simplest form of neutron detection is the count of singles to find the total neutron detection rate. Each detected neutron produces one count, and each count can be summed for the totals counts that is not dependent on location or time. This is the simplest neutron counting measurement to take but is not the most helpful in identifying or quantifying the nuclear material. A more complex measurement method that provides more useful information regarding a nuclear material sample is known as coincidence counting. Coincidence counting is a valuable neutron detection technique that provides information necessary for qualitative and quantitative

analysis of bulk nuclear samples. This technique belongs to a class of nuclear measurement methods known as nondestructive analysis (NDA) because the sample that is being analyzed is not destroyed or altered.

Neutron coincidence counting can be performed in either an active or passive manner. If the source being analyzed does not have a high rate of spontaneous fission then it is necessary to bombard the sample with neutrons from a separate neutron source in order to induce fission and measure the response. An example of material that would require active NDA is ^{235}U, as this isotope has a low rate of spontaneous fission. If the source that is being analyzed spontaneously fissions at a high rate then there is no need to bombard the sample with a neutron source because the free neutrons that result from spontaneous fission provide sufficient information regarding the quality and quantity of the isotopes in the sample. This is what is known as passive NDA and is typically used in Pu samples because of Pu isotopes have significant spontaneous fission rates.

1.2 IAEA Safeguards

The International Atomic Energy Agency (IAEA) was founded as an organization within the United Nations (UN) in Vienna, Austria in 1957. The organization's mission since its inception has been to "accelerate and enlarge the contribution of atomic energy to peace, health, and prosperity throughout the world" [2]. This noble effort to provide the opportunity for all nations in the world to prosper with nuclear energy simultaneously invokes an incredibly dangerous opportunity for countries that have the desire to acquire nuclear weapons.

In an attempt to combat the proliferation of nuclear weapons, the Nuclear Non-Proliferation Treaty (NPT) was created and put into effect in 1970 [3]. At the time of the inception of the NPT, there were five states that had already developed and were in possession of

nuclear weapons (the United States, the Russian Federation, China, France, and the United Kingdom). These five countries are identified by the NPT as nuclear-weapon states (NWS). The NPT forbids NWS from transferring nuclear weapons and the non-nuclear-weapon states from acquiring nuclear weapons. All countries that are member states of the UN have agreed to this treaty except for India, Israel, Pakistan and South Sudan (North Korea withdrew in 2003). Every country that has signed the NPT must comply with the safeguards of the IAEA to prevent development of nuclear weapons from peaceful nuclear energy.

The IAEA deploys nuclear safeguards inspectors to countries that have signed the NPT to verify nuclear declarations and ensure that they are abiding by the agreement terms. Challenges that face the inspectors include false declarations, altered samples, and other extraneous environmental factors. The inspectors can send samples back to the IAEA laboratory for destructive assay, but this process is time consuming, costly, and destroys the sample. This necessitates NDA that has been described in the previous section. An effective technology that the Agency uses for this purpose is the Active Well Coincidence Counter (AWCC) [4].

1.3 The Active Well Coincidence Counter

One of the most useful detectors for safeguards purposes is the AWCC. This device is a versatile technology to perform NDA for qualitative and quantitative characterization of nuclear materials. The AWCC is a form of a neutron detector that measures the totals neutron rate and the reals rate, which is the rate that multiple neutrons are detected within a specific time period. Varieties of neutron detectors that only detect singles are able to simply identify that there is a radiation source present but do not provide detailed information about the nuclear material that is

measured. Coincidence counters, on the other hand, allow for a measurement to provide enough data to quantify the mass of special nuclear material (SNM) in the sample that is being analyzed.

There are two types of neutron coincidence counting: passive or active. The passive technique relies on the spontaneous fission of the material being measured and active technique requires induced radiation response of the material to be detected. An example when passive neutron coincidence counting is appropriate is when analyzing plutonium samples, as even number plutonium isotopes have a large spontaneous fission rate. Active coincidence counting is required when uranium samples are being measured, as uranium (in particular ^{235}U) has a poor spontaneous fission rate. To induce a response that can be measured from a sample in active coincidence counting, an external neutron source must be used.

There are detection systems that have been specifically developed and manufactured for passive coincidence counting, as well as active coincidence counting. The AWCC is a useful and versatile tool for having the capability to perform measurements in either mode. This versatility has made the AWCC an integral tool for IAEA inspectors to determine if a State is not adhering to the terms of the NPT. It allows for the confirmation that the declared amount of fissile material is accurate or not, whether that material contains plutonium or uranium.

For AWCC active coincidence counting, a neutron source is required to induce a radiation response from the sample. The two locations for the external neutron source are shown in Figure 1.1. This cross section is of the Model JCC-51 AWCC that is manufactured by Canberra. The specifications for this model are the same as the AWCC that was used to benchmark the model that will be discussed in the following sections. If the sample being analyzed has a high enough spontaneous fission rate then these two locations for an external neutron source are left vacant.

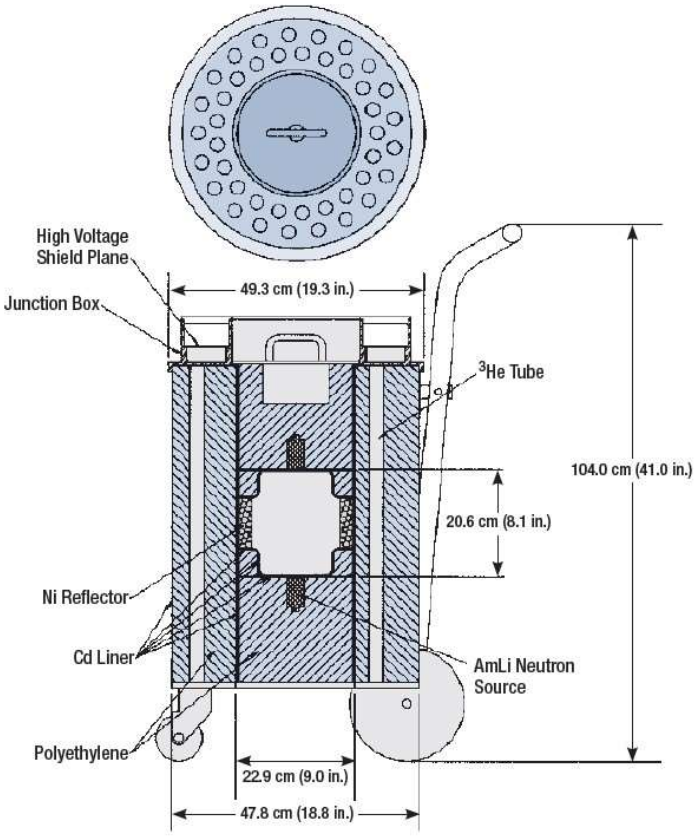

Figure 1.1 Canberra Model JCC-51 Active Well Coincidence Counter. Reprinted from [5].

Regardless of the mode that the detector is operated in, all other aspects of this detector remain constant. There are forty-two ^{3}He tubes that are surrounded by high density polyethylene (HDPE) outside of the sample area. The ^{3}He tubes are filled at 4 atmospheres absolute pressure and are 2.54 centimeters in diameter and have an active height of 50.8 centimeters. As can be seen in Figure 1.1, these tubes are organized in two concentric rings of twenty-one tubes each. There are six groups of seven tubes that relay the detection response to a JAB-01 Amplifier/Discriminator circuit board. The ability for coincidence counting is reliant upon the JSR-12 neutron coincidence analyzer, which is known as a "shift register". The shift register

circuit allows for discrimination against single counts by noting the doubles that occur within a given time frame known as “the gate length” [6].

The location that a sample is placed for measurement can be increased by removing either or both of the top and bottom plugs shown in Figure 1. Also shown in the figure is the cadmium sleeve which reduces the background influence on the measurement as well as reduces exposure to the operator of the detector.

1.4 Decline of ^{3}He Supply

An increase in demand for national security and safeguards applications of ^{3}He gas, along with industrial and medical needs (oil and gas exploration, lung imaging, laser research, fusion, etc.), has coincided with a dwindling source of tritium. Only 0.0001% of helium gas in the United States is the isotope ^{3}He. The once abundant supply of ^{3}He has continuously declined since the September 11th, 2001 terrorist attacks. Since this tragedy took place, the U.S. government has deployed neutron detectors to border crossing, both foreign and domestic, to prevent smuggling of nuclear material. This detection medium was used exclusively for this effort because it is an inert gas, has a large thermal neutron capture cross-section and good gamma ray rejection ratio.

Tritium decays radioactively at a rate of 5.5% per year in a reaction where ^{3}He, a β particle, and neutrino are the byproducts as shown in Figure 1.2.

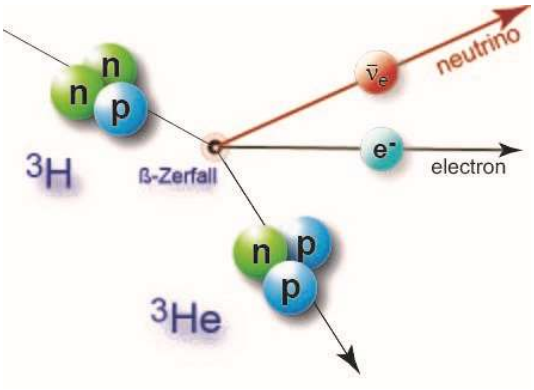

Figure 1.2 Tritium decay reaction. Reprinted from [7].

The processing of tritium is currently the sole source for ^{3}He production. There is no significant production of new tritium; the tritium stockpile has been continuously decreasing for decades due to a reduction in the number of nuclear warheads. The nuclear weapons stockpile in the United States and Russia increased drastically once the Cold War began and then continuously declined since its resolution (Figure 1.3). With the end of the Cold war the production of ^{3}He has essentially stopped.

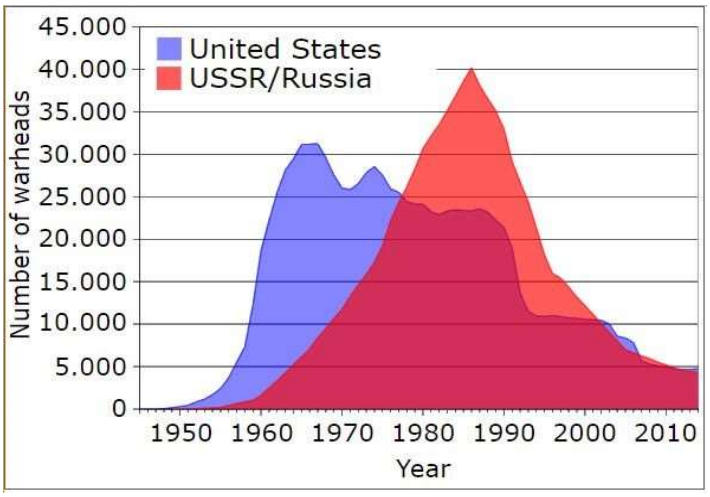

Figure 1.3 The U.S. and Russian Nuclear Weapon Stockpile. Reprinted from [8].

Production of tritium for the purpose of obtaining ^{3}He gas is cost prohibitive and not a feasible option to meet the demand for neutron detection. The United States Department of Energy (DOE) manages the production and distribution of ^{3}He through the subprogram known as the Isotope Development & Production for Research and Applications (IDPRA). This organization replenishes the tritium that decays each year and recovers, purifies, and bottles the ^{3}He that is a byproduct for distribution. The amount of ^{3}He that is generated from this program per year is approximately 8,000 liters [9]. The unsubsidized cost of producing tritium for nuclear weapons is between $84,000 and $130,000 per gram, which corresponds to a cost between $11,000 and $18,000 per liter of ^{3}He [10]. In addition to the high cost, the quantity produced is not enough to meet the demand for ^{3}He gas and has projected the supply will continue to decline, as seen in Figure 1.4.

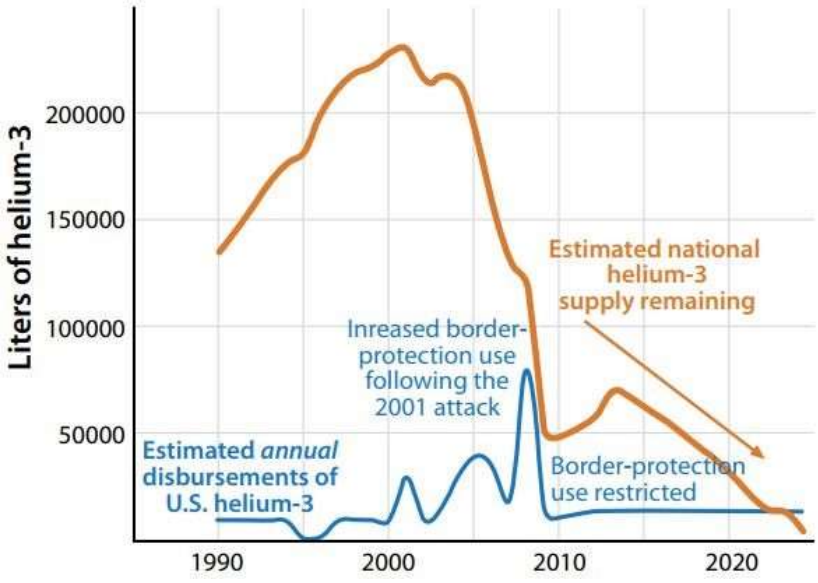

Figure 1.4 Helium-3 Stockpile Projection. Reprinted from [11].

The sharp decline in Figure 1.4 in 2009 is responsible for the increase in price. The marginal price of ^{3}He gas was historically $100 to $200 per liter until this rapid decline in availability. With meager production of tritium in the United States compared to the increase in use, and Russia terminated exports of approximately 25,000 liters per year of ^{3}He in 2010, the price has been greatly affected. In 2009 the DOE started to ration ^{3}He and the cost rose all the way to $2,000 per liter in at a DOE auction in 2010 [10].

1.5 Potential Replacement Detection Media

The combination of increased demand for neutron detection and decreased supply of ^{3}He has made an alternative detection medium with acceptable capabilities imperative. There are currently four unique technologies that are at present available commercially as prospective replacements for ^{3}He. The four possible replacements are boron trifluoride (BF_3) filled proportional counters, lithium-loaded glass fibers, coated non-scintillating plastic fibers, or boron-lined proportional counters. Each of these potential replacements for ^{3}He come with their own set of challenges. As seen in Figure 1.5, ^{3}He has the best thermal neutron cross section compared to the alternative detection mediums.

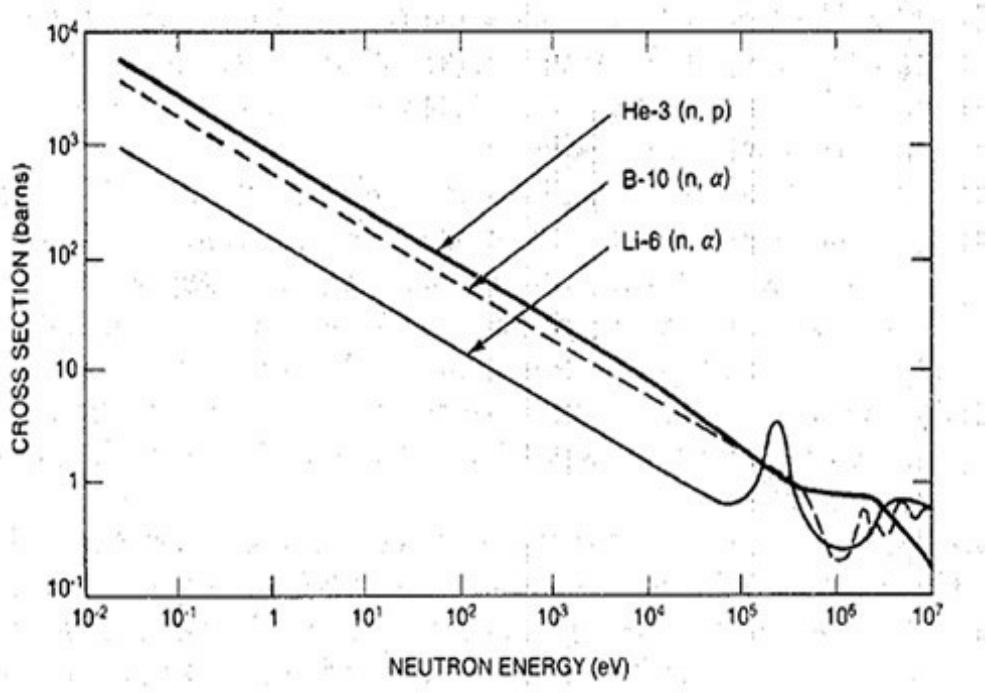

Figure 1.5 The cross-section of ^{3}He, ^{10}B, and ^{6}Li as a function of incident neutron energy. Reprinted from [12].

There are various disadvantages for each of the neutron detection technologies that do not rely upon ^{3}He. For example, the aforementioned BF_3 based detection system has a cross-section of roughly only 70% to that of ^{3}He. Additionally, BF_3 gas is toxic, requires a complex process to be purified, degrades over time, and is corrosive to the enclosure in which the gas is encased. This detection alternative would also come with the inconvenience of being transported in compliance with strict Department of Transportation shipping requirements, whereas ^{3}He is an inert gas and fewer regulations are required for shipment.

Lithium-loaded glass fibers may have the benefit of being less dangerous than BF_3, but it is apparent from Figure 1.5 that this medium has a significantly smaller neutron absorption cross section than both ^{3}He and BF_3. Lithium-loaded glass fibers produce a signal when the ^{6}Li

absorbs a thermal neutron and the charged particles from the $^{6}Li(n,\alpha)^{3}H$ reaction produce light in the glass fibers. The fibers then conduct the light to photomultiplier tubes. This additional medium along with the inferior neutron absorption cross section creates a necessity for more material which would significantly increase the footprint of the AWCC in order to match the efficiency of the original AWCC system with ^{3}He. Coated non-scintillating plastic fibers [$^{6}Li/ZnS(Ag)$] require plastic wavelength shifting fibers to pass light to photomultiplier tubes as well. Both of these technologies show promising results in replacement neutron detection for a more spacious detector (such as a Radiation Portal Monitor) but would require too much material to be feasible for AWCC replacement detection medium.

Boron-lined proportional counters appear to be the most promising potential replacement for ^{3}He in an AWCC. This detection medium has the same thermal neutron absorption cross section as BF_3, which is superior to that of ^{6}Li based detection systems, while not having the explicit danger the toxic gas of BF_3. Because boron-lined detection systems are not gaseous as BF_3, there is a need to increase the amount of ^{10}B in the system. Boron-lined tubes will not be able to come close to the efficiency of the original ^{3}He system, but smaller boron lined straws within the confines of the dimensions of the aluminum tubes that contain ^{3}He gas could be a possible solution. In this work an increase in the number of straws will be experimented with in an attempt to raise the efficiency of boron-lined tubes to meet the standard set by AWCC systems with ^{3}He gas as the detection medium.

2. RADIATION DETECTION SIMULATIONS

An AWCC is a complex radiation detection system that can produce results which vary significantly from minor changes in its design. In order to mitigate costs in producing an alternative, many iterations of different types of designs must be simulated rather than actually manufactured. Once a thorough analysis has been done on each variable, the optimal simulation may be physically built. In order to ensure the results of the simulations are valid, there must be a baseline model which has been validated with experimental data.

The use of a system model makes it possible to find a system with the highest possible performance within the stated design constraints. An attempt to maximize performance is confirmed by running many iterations with minute changes to the model to confirm predictions of system performance. By using the Monte Carlo method, it is possible to simulate individual particles and note their average behavior to determine how particles within the system act. The Monte Carlo method used in this research is a simulation of the spatial transport of neutrons between certain types of events. A random number generator to sample each type of event during the neutrons lifetime is used within this method to sample randomly (using the cross-section files for the materials that are used) the probability distribution that are built into the software. Any additional particles that are generated from the initial model through interactions are stored for future analysis. The simulations conducted during this research were all executed with the Monte Carlo method with the evaluation of performance focused on the Figure-of-Merit (FOM), which is the square of the intrinsic efficiency (ε^2) divided by the die-away time (τ). The τ is the time that has passed from neutron emission to detection. The FOM is the industry standard used to evaluate coincidence counter performance, including the AWCC [13].

2.1 MCNPX Simulations

The Los Alamos National Laboratory (LANL) developed Monte Carlo N-Particle transport code (MCNP) was used for this research to simulate the existing and potential AWCC configurations [14]. Electron, neutron, and photon transport are all possible to simulate with MCNP. MCNPX was released in April 2011 with the added feature capable of the transport of heavy charged particles (α and tritons) [15]. MCNPX v.2.7.0 was used for the simulations conducted in this research effort because of the nature of the neutron interaction and detection with the boron-lined tubes and straws. Neutrons react with the ^{10}B lining and produce charged particles from the $^{10}B(n,\alpha)^{7}Li$ reaction that are responsible for the signal produced in the detector. This version of the software allows for transport and tallying of the heavy charged particles in the simulations.

In order to simulate a detection system in a realistic manner, the characteristics of the neutron capture reaction and the signal generation must be considered. An AWCC which relies upon ^{10}B lining operates in a two-step detection process because the neutron capture material and the signal generating material are different. The ^{3}He system has the benefit of the material that captures neutrons is also the material that generates the signal, the detection efficiency can be found in one step by recording the number of captures. This means that an F4 tally can be used (in addition to a multiplier card to specify capture reactions) to simulate the number of neutrons that are captured in the ^{3}He gas.

In the system which relies on boron-lined tubes or straws, there is an additional step to compute the signal that will be generated. Neutrons must be captured in the lining and then the reaction products must escape that material and cross into the signal generating gas. The neutron captures can be tallied with the F4 tally, but this will cause an over estimate of the signal

generation. In order to produce a more precise estimate, the reaction products produced must be tracked as they cross into the signal generating gas. Heavy ions must be tracked (as the reaction products of the neutron capture in the boron lining results in ^{7}Li and α particles), which is an added feature in the MCNPX v2.7.0 code that was used. This version of MCNP grants the ability to require correlation of the reaction products with the correct two-branch Q-values for neutron capture reactions in ^{10}B [15]. The utilization of F8 tallies allows for the accurate simulation of the energy that is given off by the reaction products in the signal generating gas, as it is a pulse height (PH) tally. This tally is completed at the end of the particles' lifetimes in the simulations. Deposited energy from specified areas of the AWCC are recorded. This is done when the energy of the reaction products as they enter the signal generating gas is compared to the energy as they leave the area or goes below the cutoff energy in the simulation. This defining trait of the F8 tally means that the net energy deposition of a particle created within the same volume that it is captured in would be equal to 0. In order to ensure validity of the simulations, a measured experimental response must be compared to the simulation of the same system and source specifications.

3. HELIUM-3 MODEL

An input file was created to model the AWCC that is located at PNNL in the 300 Area shown in Figure 3.1. This AWCC was manufactured by a small startup company called Jomar Systems between 1975 and 1977 for LANL. Jomar Systems was later acquired by Canberra Industries in 1990. The system at PNNL that was used for benchmarking the model has identical specifications as the JCC-51 model of the AWCC that is currently manufactured by Canberra Industries [5].

Figure 3.1 JOMAR AWCC at PNNL (later manufactured as the JCC-51 by Canberra).

The AWCC with ^{3}He as the detection medium was designed to the specifications discussed in Section 1.3 of this document. The ^{3}He gas acts as both the neutron capture material and the signal generating material, as seen in Figure 3.2. This characteristic of the original AWCC allows for the simulation to be coded in MCNPX as a one-step process. This allows for the input file to utilize an F4 tally to predict the signal generating efficiency.

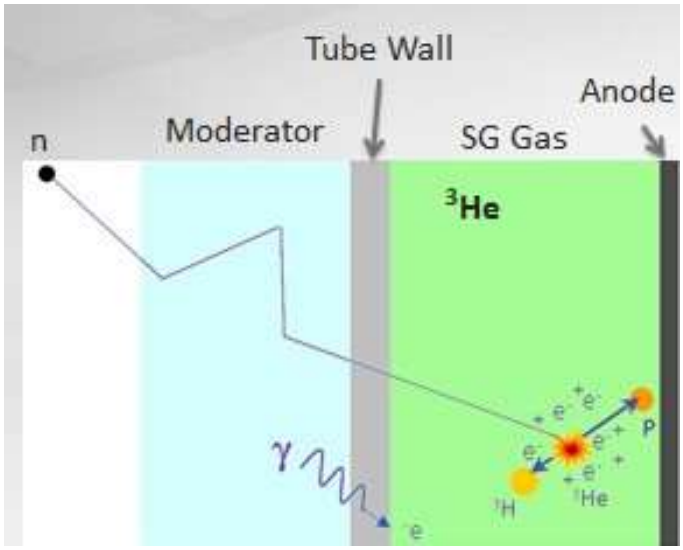

Figure 3.2 Helium-3 detection reaction.

The neutron capture reaction in ^{3}He has a cross section of 5330 b and produces a proton and a triton. This thermal neutron reaction has a Q-value of 0.764 MeV and is released by oppositely directed reaction products with energies of KEp = 0.573 MeV and $KE_{^{3}H}$= 0.191 MeV. The pertinent equations for this detection reaction can be seen in Equation 3.1 and Equation 3.2.

$$\mathbf{n + {}^{3}He \rightarrow H + {}^{3}H} \tag{3.1}$$

$$\mathbf{KE_{p} + KE_{^{3}H} = Q} \tag{3.2}$$

To begin the simulations in MCNPX, an input file that was designed by Commissariat L'Energie Atomique (CEA) based on the AWCC was translated from French to English and updated to the specifications of the detector used at PNNL [16]. This model is of the original AWCC configuration with ^{3}He as the detection medium and is shown in Figure 3.3.

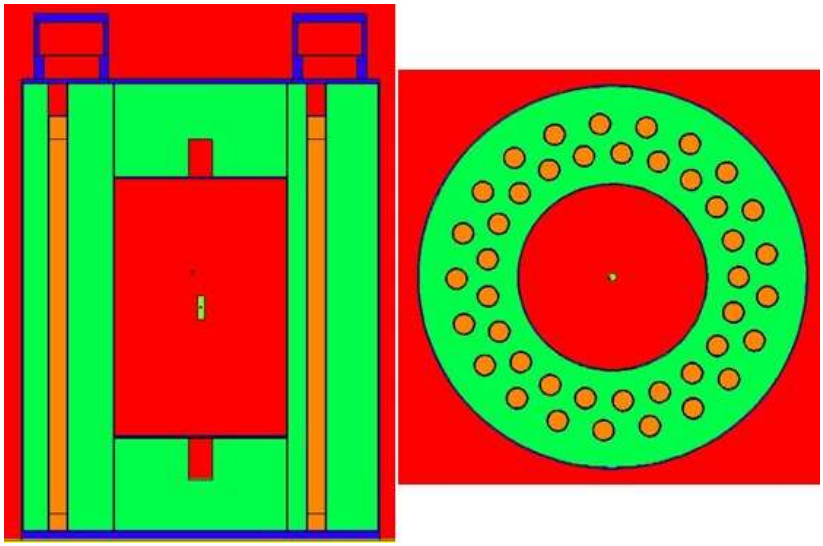

Figure 3.3 Side and top down view of ^{3}He based AWCC.

3.1 AWCC with ^{3}He Model Results

For each of the simulations run in this research, the die-away time (τ) for all of the models was computed by quantifying the number of neutrons that were captured per a time interval and then using an exponential regression to fit the results. The neutron capture tallies were taken in twenty 5 μs bins, from 0 to 100 μs. The results of the ^{3}He system are shown in Figure 3.4 for the MCNPX pulse height tally. Figure 3.4 shows the total count efficiency (TCE), which is the percentage of neutrons emitted that elicited a signal in the detection system. The TCE is the sum of all the points that make up the line in the figure. Features of the energy

spectrum shown in Figure 3.4 are a result of the kinetic energy of each of the reaction products and are indicated by yellow diamonds. The Q-value of the reaction is represented by the red square at 0.764 MeV.

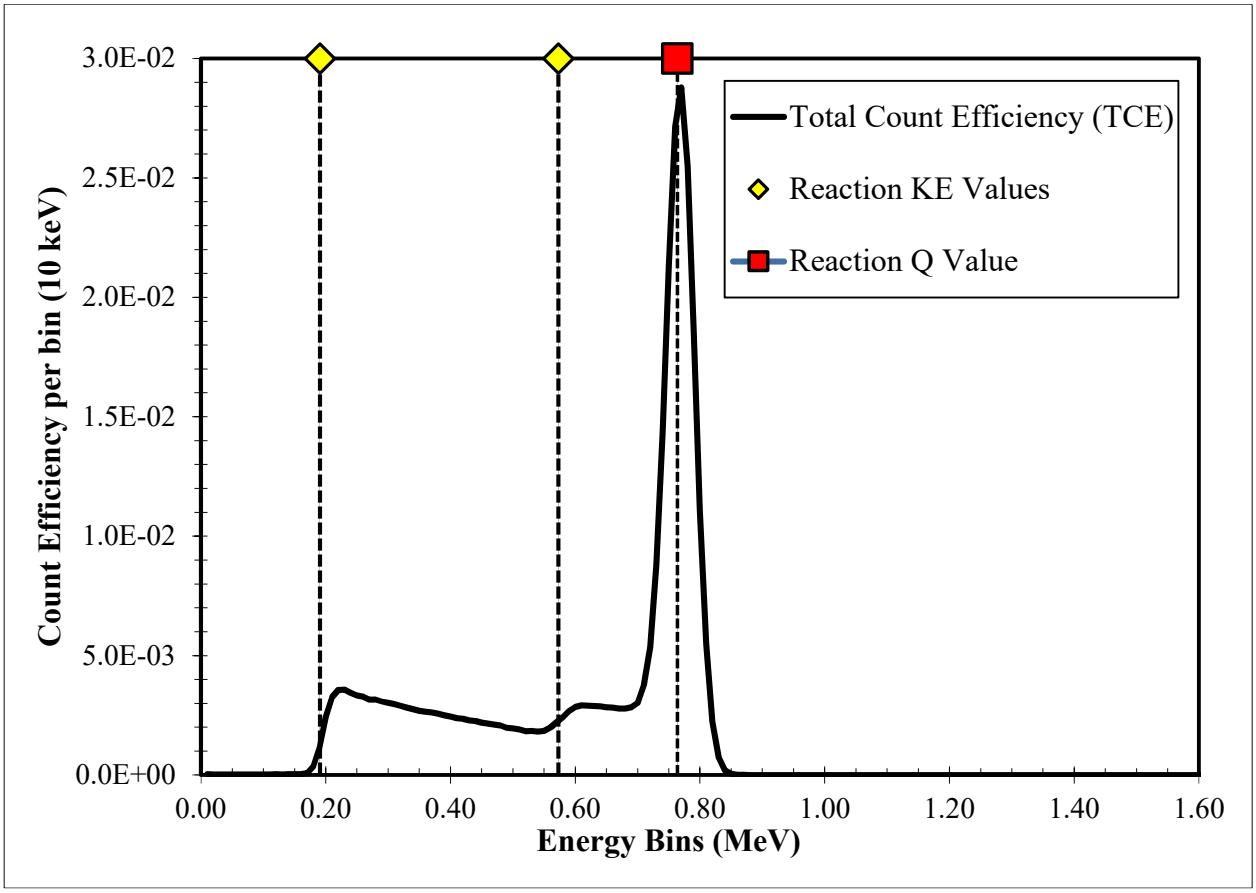

Figure 3.4 AWCC with 42 Helium-3 Tube Pulse-Height Light Distribution.

The pulse-height spectrum from the ^{3}He system gets its shape from the kinematics of the reaction process. The full-energy peak at the Q-Value of 0.764 MeV occurs because it is the collection of the kinetic energy of both of the reaction products (proton and triton). In the instance that one of the two particles escape without depositing all of its energy or is absorbed in

the tube lining, less energy will be deposited into the gas. This phenomenon explains the small low-energy tail peaks that appear just after the reaction kinetic energy values that are indicated by the yellow diamonds in Figure 3.4. In comparison to the typical pulse-height spectrum from a ^{3}He proportional counter shown in Figure 3.5, the behavior of the model appears to be reasonable. The only difference in behavior between the two figures appears at the low energy end of the spectrum. This is because the input file in MCNP specified to begin the tally of energy deposition at 0.1 MeV in order to intentionally eliminate the peak on the far left of the spectrum in Figure 3.5, which is known as pulse shape discrimination (PSD). This peak is a result of low-amplitude events such as gamma ray interactions and electronic noise.

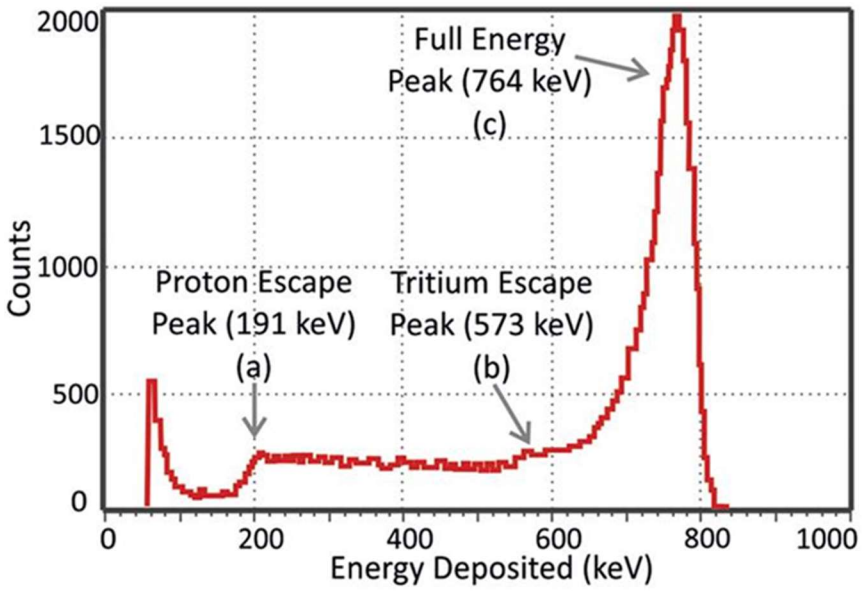

Figure 3.5 Pulse-height spectrum for thermal neutrons detected by a ^{3}He filled counter. Reprinted from [17].

Table 3.1 AWCC with ^{3}He simulation results

Helium-3 Gas Filled GERS Tubes							
Diameter (cm)	Pressure (atm)	# Tubes	^{3}He (g)	Total Captured	TCE	τ (μsec)	FOM
2.54	4.00	42	8.90	30.9 ± 0.02%	30.9 ± 0.02%	52.2 ± 0.0206	18.291 ± 0.007

The performance values associated with the Pulse-Height Distribution in Figure 3.4 for the ^{3}He AWCC is seen in Table 3.1. The τ in this table was found by fitting an exponential regression, as discussed previously, to the ratio of counts to neutrons emitted in 5 μs bins. This method was used because there is no way to generate a τ value in MCNPX, but this technique provides an estimate. There are no error bars shown on any of the figures from the simulation results. This is because the error bars are too small and are being obscured by the data points. The simulation results in this report passed the MCNPX tests and the number of particles simulated was high enough to have a statistical uncertainty less than 1%. The results and regression fit are shown in Figure 3.6.

The equation for the exponential regression fit is shown in Figure 3.6. This regression has an R^2 value of 0.9999. This precision is attributed to the nature of the ^{3}He detection system. Because the signal generating medium and neutron capture medium are the same, the total neutrons captured and the TCE are also the same. The percentage of counts per emitted neutron for the specified time intervals can be fit with a regression to calculate the τ with the highest level of confidence because of this characteristic.

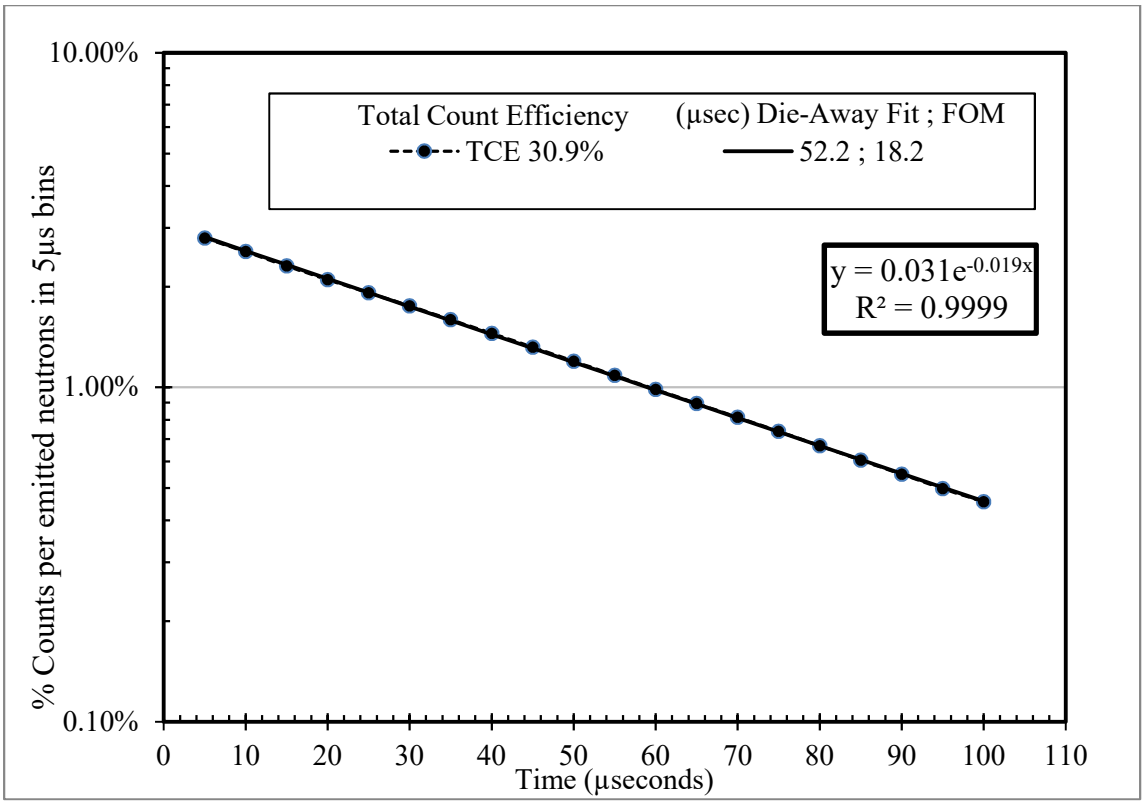

Figure 3.6 AWCC with 42 Helium-3 Tubes Die-Away Time.

The TCE of the AWCC with ^{3}He of 30.9% will be compared to the measured data from a source of the same modeled activity. The 18.29 FOM is the standard which the BCS system is intended to meet in order to be a viable replacement for the original ^{3}He AWCC.

3.2 Benchmarking the ^{3}He Model

The AWCC model was validated by comparing the simulation results to experimental data. The measured values for the ^{3}He AWCC are seen in Table 3.2. The efficiency has been modeled for single neutron captures, as this efficiency will indicate the alternative AWCC model's ability to match the coincidence count efficiency of the AWCC with ^{3}He.

Table 3.2 Measured singles counts with statistical error.

	Source	Singles	$\sigma_{singles}$
RMT#	BG	9.481	0.13
68118	^{252}Cf	16795.5	5.626

The certified AWCC source emitted $5.610 * 10^4$ n s^{-1} and was counted for the same amount of time as the simulations. This data gives a TCE of 29.9%. This value shows that the simulation is producing a higher rate of detection of neutrons (shown in Table 3.1), but because it is within 1% of efficiency, the model is considered to be a valid representation of the system and has proved to be a sufficient template for further exploration of alternative detection media.

4. REPLACING HELIUM-3 WITH BORON-10

The replacement of ^{3}He with ^{10}B as the detection medium poses the obvious question of just how much ^{10}B will be required to meet the standard of total count efficiency (TCE) set by the original AWCC setup. To assess how much ^{10}B would be required to match this TCE, a simple calculation was used. Before the investigation of BCS in an AWCC configuration, ^{10}B-lined tubes were evaluated. The reason for this is that it is a simpler modeling process and serves as a foundation to improve upon. In the input file of the ^{3}He system, there is one master tube which is replicated 41 times throughout the system. It is relatively quick to edit the ^{3}He master tube in the input file to represent a ^{10}B-lined tube that is replicated 41 times. A model with seven straws within a tube that is mirrored 41 times adds a level of complexity.

Before the simulation was run, a rough estimation of the amount of ^{10}B required to result in the same number of neutron capture reactions in the ^{3}He system was calculated to serve as a comparative number. Two variables and one assumption were used to calculate the approximate number of ^{10}B-lined tubes needed to produce the same number of in-gas counts as the original ^{3}He system. These variables were the number of moles in each system (42 tubes) and the ratio of thermal neutron capture cross sections. The total number of moles in each system were determined from the tube specifications and the ratio of thermal neutron capture cross sections is shown in Equation 4.1.

$$\left(\frac{^{3}\mathbf{He}}{^{10}\mathbf{B}} = \frac{\mathbf{5330b}}{\mathbf{3840b}}\right) \tag{4.1}$$

The assumption that had to be made was that only one of the two reaction products from the ^{10}B capture reaction will enter the proportional gas. This assumption is made because the two reaction products of the detection reaction travel in opposite directions. Since the ^{10}B is only in

the lining of the tubes at best only one of the two reaction products per capture event will be directed towards the center of the tube and into the proportional gas. To take into account that only one of the two reaction products will enter the gas, a factor of $\frac{1}{2}$ was used.

The calculation of the approximate number of ^{10}B-lined tubes (as opposed to the thin BCS) required to produce the same in-gas counts was found to be 194 tubes. This number was then compared to the output file produced from the simulation of the AWCC with the same dimensions as the JCC-51 and GERS tubes, only with a 2.5μm lining of 96% enriched $^{10}B_4C$ discussed in the previous section. This calculation and comparison was done as an initial step on finding a suitable alternative to the ^{3}He tubes in the AWCC. The reason for this is that the GERS ^{10}B-lined tubes operate with the same reaction scheme as the BCS and have been proven as a useful neutron counting medium over a long operating history that spans 70 years [18].

The thermal neutrons that are captured in the lining result in secondary particles traveling isotropically in the opposite direction. This reaction is the $^{10}B(n, \alpha)^7Li$ reaction in Equation 4.2.

$$n + {}^{10}B \rightarrow {}^{4}He\ (\alpha) + {}^{7}Li \tag{4.2}$$

This reaction leaves the ^{7}Li ion in an excited state 94% of the time with Q = 2.310 MeV, with kinetic energies of ^{7}Li and α being 0.840 MeV and 1.470, respectively. For the minority of the reactions (~6%) the ^{7}Li will be left in ground state and Q = 2.792 MeV and the initial kinetic energies are 1.015 MeV and 1.777 MeV, respectively. Figure 4.1 illustrates the nature of the capture reaction that takes place in ^{10}B-lining in this detection system. The example portrayed in Figure 4.1 shows the ^{7}Li atom escaping the tube while the α-particle is directed into the

proportional gas. It should be noted that α-particle could escape the lining and the ^{7}Li atom could enter the gas to deposit its energy as well. The illustration is intended to represent the impossibility of both reaction products simultaneously entering the proportional gas to deposit their energy, which prevents a full collection of the Q-value.

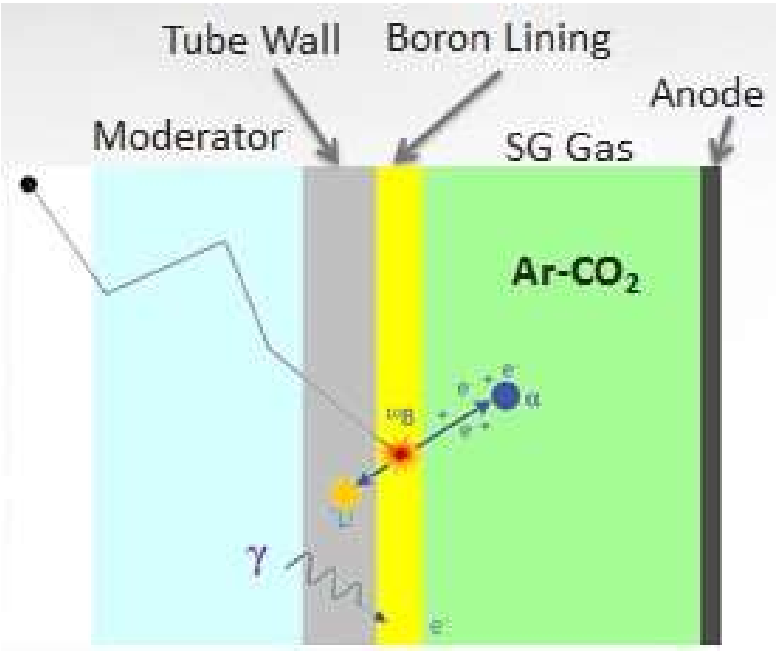

Figure 4.1 Neutron capture reaction in Boron-10.

The neutron thermal capture cross-section ratio of ^{10}B to ^{3}He is 0.72 and there are 0.93 moles of ^{10}B in the ^{10}B-lined AWCC compared to 1.55 moles of ^{3}He in the original AWCC. It can be calculated with the ratio of moles of material, the ratio of cross sections, and the original system TCE of 30.9% that the upper constraint on the TCE of this simulation is 20.7%. It is much more probable that the TCE will be even less for this simulation because of the nature of the reaction, as previously discussed.

4.1 AWCC with ^{10}B-Lined Tubes Results

The first simulation was created to determine the accuracy of the approximation derived in the previous section. Each of the 42 ^{3}He tubes were replaced with GERS tubes of the same dimensions that were lined with 2.5μm of ^{10}B and filled with 0.70 atm of $ArCO_2$ gas inside of identical aluminum outer casing in order to maintain the same HDPE footprint. The same model of ^{252}Cf source and number of particles were simulated to compare the total number of captures, TCE, and τ in order to compare the FOM of each system. The resulting pulse-height distribution is shown in Figure 4.2.

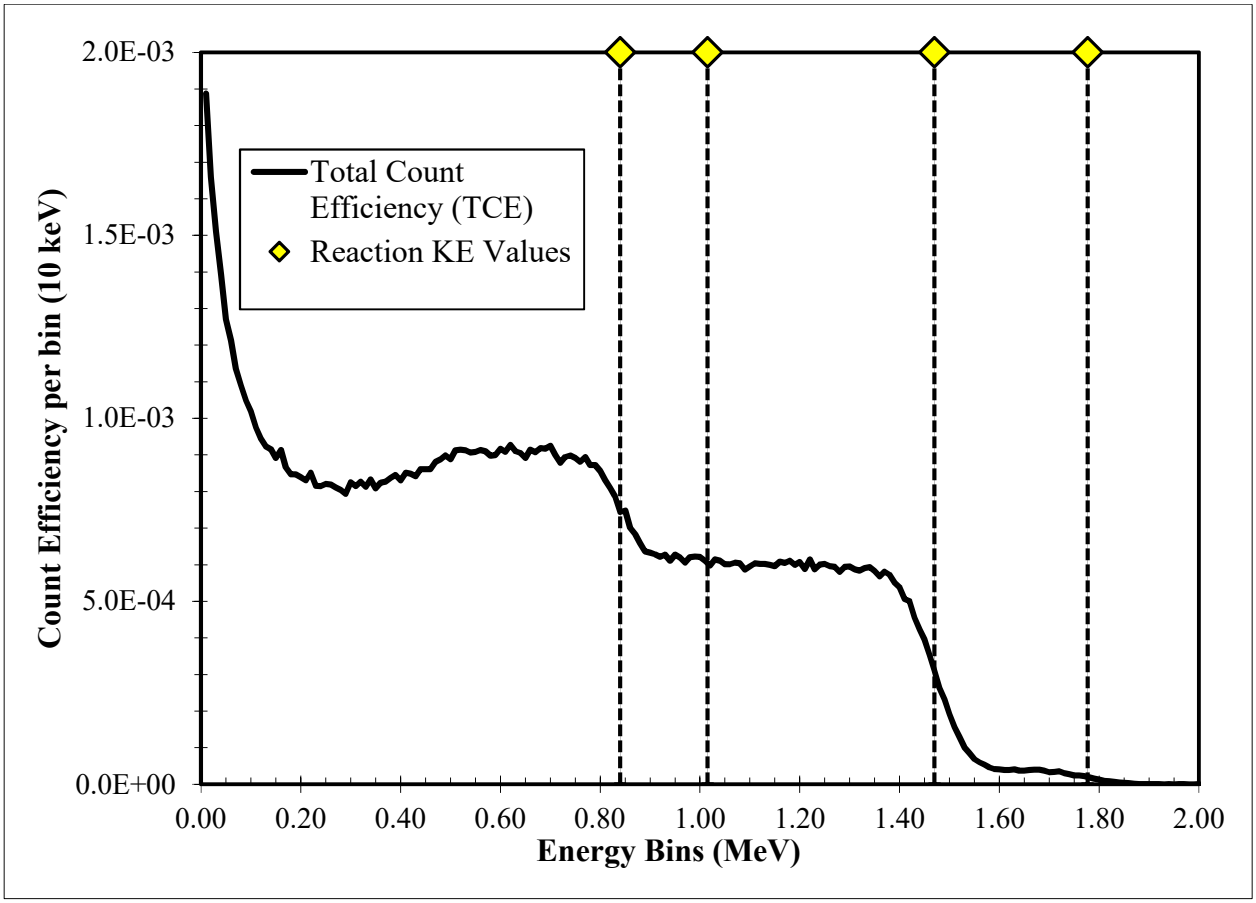

Figure 4.2 AWCC with 42 BL Tubes Pulse-Height Light Distribution.

The ^{7}Li atom and α-particle that result from a neutron capture in the ^{10}B-lining travel in opposite directions, which accounts for the spectrum shape of Figure 4.2. This constraint of the geometry prevents a full Q-value peak, unlike in the ^{3}He pulse-height light distribution. The two potential outcomes of a neutron capture reaction in the ^{10}B-lining are either the ^{7}Li atom or α-particle enter the proportional gas to deposit energy. Regardless of which reaction product enters the gas, some of its energy will be lost in the lining of the tube before energy can be deposited in the proportional gas. The kinetic energy values of 0.84 MeV for the ^{7}Li atom and 1.47 MeV α-particle are the threshold energies up to which each reaction product can deposit energy 94% of the time. For the remaining 6% of the time, the kinetic energy values of 1.015 MeV and 1.777 MeV are the maximum energy to be deposited in the gas from the ^{7}Li atom and α-particle, respectively. The four kinetic energy values of interest are seen in Figure 4.2 to be represented by yellow diamonds.

In comparison to the typical pulse-height spectrum from a ^{10}B-lined proportional counter shown in Figure 4.3, it appears the model produced an output as expected. Both the model and example pulse-height spectrum appear to have a sum of two flat distributions that correspond to each of the two reaction products that result from the neutron capture reaction. The drop downs occur just before each kinetic energy value because that is the maximal amount of energy that each reaction product can give off in the proportional gas. Figure 4.3 does not show the 6% possibility of the ^{7}Li atom and α-particle depositing up to 1.015 MeV and 1.777 MeV, respectively, because of the rarity of this occurrence. Despite this difference in the two pulse-height spectra, the overall behavior of each figure provides assurance that the model is behaving as expected.

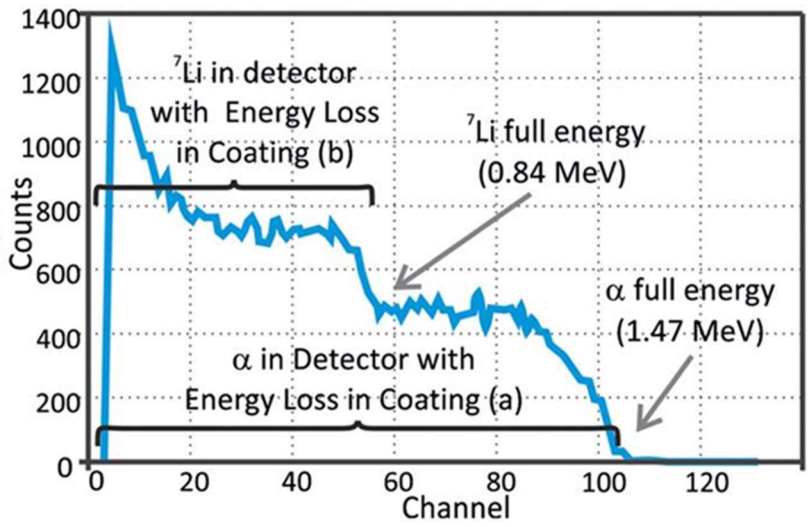

Figure 4.3 Pulse-height spectrum for thermal neutrons detected by a ^{10}B-lined counter. Reprinted from [17].

The performance values associated with the PH Distribution in Figure 4.2 for the AWCC with ^{10}B-lined tubes is shown in in Table 4.1. The τ in Table 4.1 was found by fitting an exponential regression, just as in the previous section with the ^{3}He system, to the ratio of counts to neutrons emitted in 5 μs bins. The results are shown in Figure 4.4.

Table 4.1 AWCC with ^{10}B-lined tubes simulation results.

Boron-10 Lined GERS Tubes						
Diameter (cm)	**# Tubes**	**^{10}B (g)**	**Total Captured**	**TCE**	**τ (μsec)**	**FOM**
2.54	42	10.15	24.0 ± 0.02%	11.7 ± 0.01%	93.3 ± 0.07	1.47 ± 0.0002

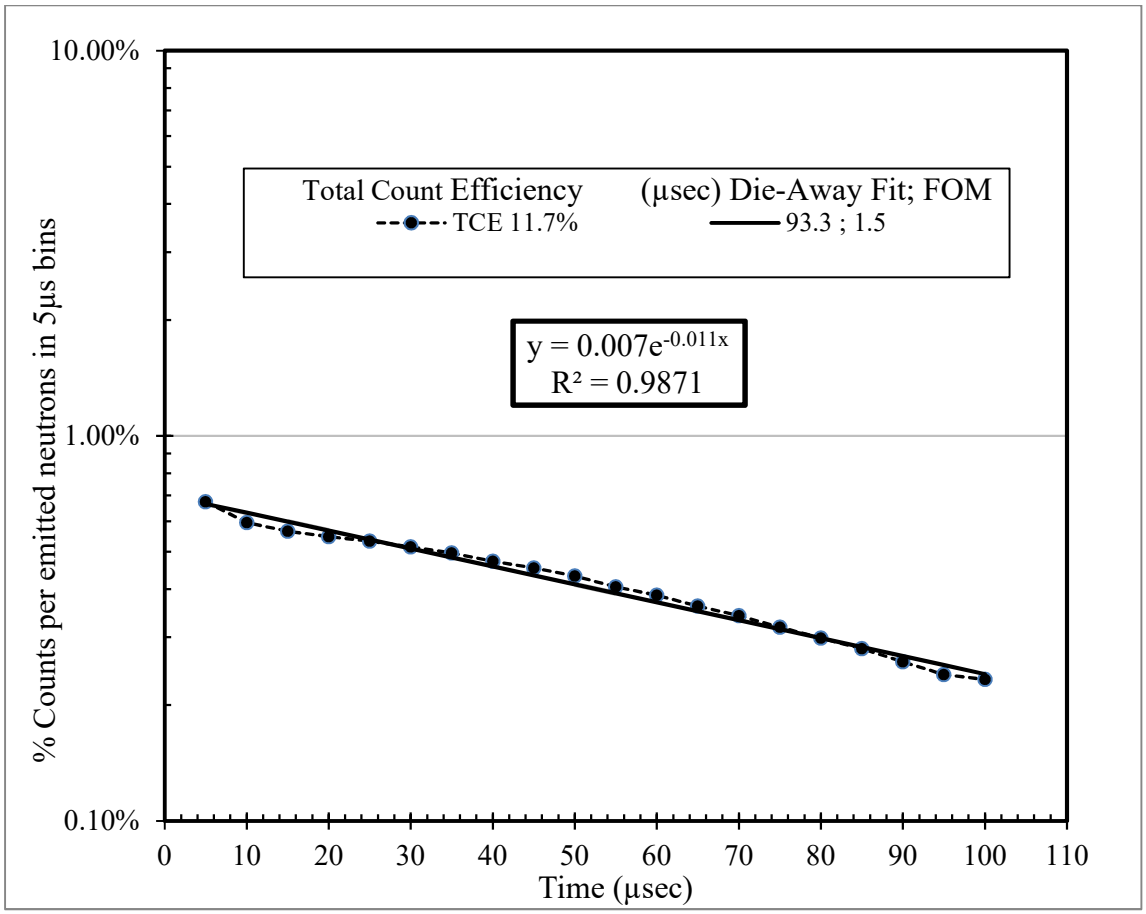

Figure 4.4 AWCC with 42 ^{10}B-Lined Tubes Die-Away Time.

The shape of the Figure 4.4 appears to be reasonable. Oscillation of the TCE in the figure is observed due to the nature of the detection system used. As mentioned previously, the ^{10}B-lined detection system operates with a different capture medium and proportional gas. Depending on the depth in the lining of the neutron capture, some reaction products give off more energy and take more time to reach the proportional gas to elicit a signal. This characteristic of a two-step detection system could contribute to more erratic behavior of the plot that represents the percentage of neutrons resulting in counts versus time. While the R^2 value of

0.9871 is not as precise as in the ^{3}He case, it is high enough to show validity of the calculated τ value.

The total captured neutrons and TCE of the ^{3}He system are identical, whereas the TCE is 12.3% less than the total captured neutrons in the ^{10}B-lined simulation. This was to be expected and accounted in the rough approximation of the amount of ^{10}B-lined tubes needed to match the TCE of the original system with ^{3}He. The factor of ½ was used, as explained in the previous section, as a factor to account for only half of the reaction products entering the gas and the potential for wall effects to reduce the signal being generated. Because the TCE in the ^{10}B-lined case was less than half of the total captured neutrons, this indicates that either the wall effects will have more of an impact than anticipated or that the 2.5 μm lining thickness is not the optimal level of thickness for the reaction products to escape into the gas. These phenomena will be further explored in the BCS cases as the lining thickness will be iterated in simulations, as will the diameter of the straws.

5. BORON COATED STRAW TECHNOLOGY

The development of boron-coated straw (BCS) technology was proposed as a potential solution to the dwindling ^{3}He supply. This technology has the benefit of the significantly lower cost in comparison to ^{3}He, while increasing the low efficiency and FOM of the standard ^{10}B-lined tubes. Proportional Technologies, Inc. has developed this alternative detection medium that utilizes thin copper straws that are 50.8 μm thick and coated inside with an even thinner ^{10}B-enriched boron carbide ($^{10}B_4C$). This thin layer of $^{10}B_4C$ has been used as a coating from "about 0.5 μm to about 3 μm thicknesses" per the patent assigned to Proportional Technologies, Inc. [19]. The schematics for a signal straw is shown in Figure 5.1.

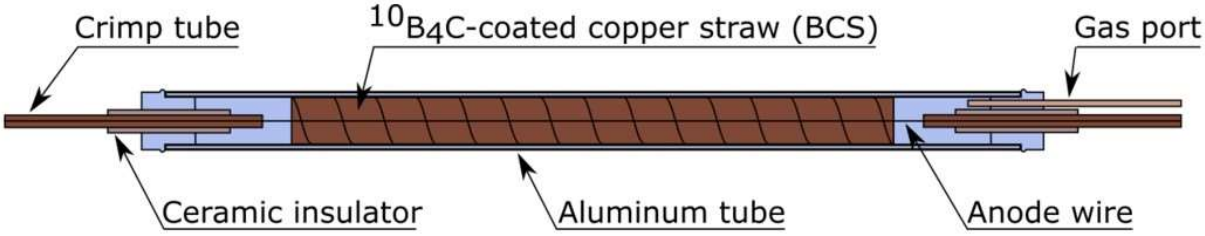

Figure 5.1 Proportional Technologies, Inc. developed Boron-Coated Straw. Reprinted from [20].

This alternative neutron detection medium is not only significantly cheaper than ^{3}He and other ^{10}B based detection systems, but boasts multiple other benefits. The BCS have many-times faster electronic signals, do not require high pressurization (0.70 atm), have improved gamma ray rejection, do not contain toxic or flammable gases, and have easier serviceability [21].

The reaction that takes place in the lining is the same process discussed in the ^{10}B-lined tube case, with the same reaction products and initial kinetic energies. Each of the reaction

product's potential distance traveled radii is shown in Figure 5.2. This figure shows only the one layer of boron, but as the straws that are being modeled vary in diameter, it is expected that the "wall effects" will be a detractor from TCE as the diameter decreases.

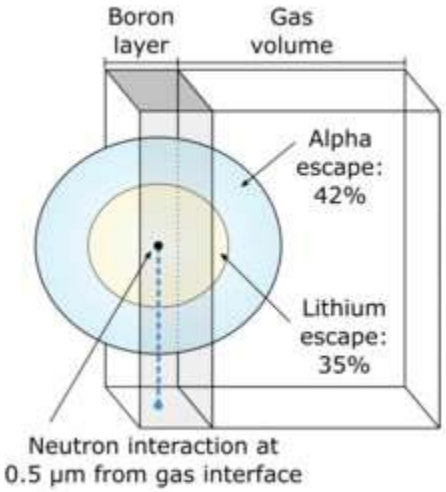

Figure 5.2 Boron-Coated Straw detection radii. Reprinted from [20].

The likelihood that the reaction product that enters the proportional gas and only loses some of its energy in the gas before hitting the opposing wall increases as the distance to the wall opposing wall decreases. This effect could distort the observed signal and counts would be lost from the signal below the low energy cutoff in the event that the only reaction product that enters the gas does not deposit sufficient energy in order to elicit a signal [22].

5.1 Boron-Coated Straw Implementation

To maintain similar geometries for the previous models, arrays of the BCS were placed inside the same GERS aluminum tubes as the ^{3}He gas and ^{10}B-lined proportional counters. To begin the simulations with BCS, the standard seven straw bundle was modeled as shown in Figure 5.3.

Figure 5.3 Current backdrop on the Proportional Technologies, Inc. website of a seven BCS bundle in 1 inch diameter aluminum tubes.

From this configuration, the straws diameter and thickness were varied in an effort to find the optimal FOM possible and fit into the original AWCC footprint. The patent for BCS states that lining thickness can vary, depending on application, from "about 0.5 µm to about 3 µm". Because of lack of specificity in the description of the lining, coupled with the absence of any publications using 0.5 µm or 3 µm thicknesses, the simulations focused on 1 µm to 2.5 µm thick lining in 0.5 µm increments. Both of these lining thicknesses were found to have been researched by Proportional Technologies, Inc. and PNNL, respectively [23, 22]. The cross

section of the AWCC and individual GERS tube is shown in Figure 5.4 with 5 mm diameter straws of 2.5 μm thick lining as an example for reference.

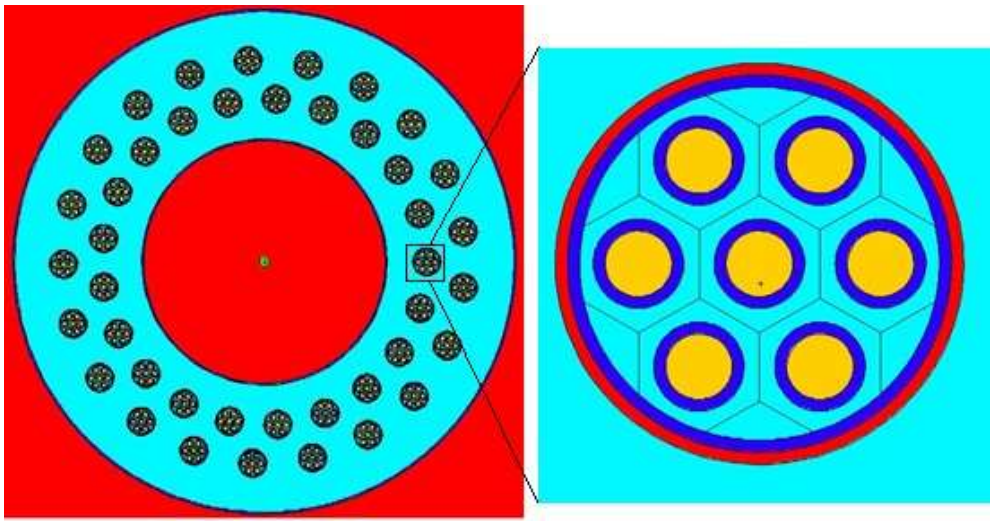

Figure 5.4 GERS Tube with seven 5 mm diameter BCS (2.5 μm thick lining).

5.2 Results

This research effort was conducted in such a way that the predicted behavior of each set of simulations would show an increase in FOM as the diameter was increased. The results of all simulations run with seven BCS per GERS aluminum tube, with varying lining thickness, are shown in Table 5.1. The analysis of the data proceeds in the same manner as the simulations were run. To begin, the smallest diameter straws with the four specified lining thicknesses were simulated followed by the next set with a diameter increase of 1 cm and the same four lining thicknesses, and so on. This pattern continued until 8 mm diameter straws could not fit within the GERS aluminum tube, so 7.8 mm diameter was used. This was the final set of simulations

run with seven straws per tube. Results for the twenty simulations with varying boron lining thickness and diameters are shown in Table 5.1.

Table 5.1 AWCC with BCS of varying diameter and lining thickness.

Diameter (cm)	Thickness (µm)	# Straws	^{10}B (g)	Total Captured	TCE	τ (µsec)	FOM
0.78	1.5	294	11.96	26.3 ± 0.02%	17.5 ± 0.01%	72.0 ± 0.05	4.253 ± 0.0007
0.78	2	294	15.95	28.5 ± 0.02%	16.2 ± 0.01%	62.2 ± 0.08	4.219 ± 0.0008
0.7	1.5	294	10.72	25.6 ± 0.02%	17.1 ± 0.01%	73.0 ± 0.07	4.005 ± 0.0007
0.7	2	294	14.29	27.9 ± 0.02%	15.9 ± 0.01%	63.7 ± 0.11	3.969 ± 0.0008
0.78	2.5	294	19.93	30.0 ± 0.02%	14.9 ± 0.01%	56.1 ± 0.11	3.957 ± 0.0010
0.7	2.5	294	17.86	29.5 ± 0.02%	14.7 ± 0.01%	57.6 ± 0.14	3.751 ± 0.0010
0.78	1	294	7.97	22.9 ± 0.02%	17.9 ± 0.01%	90.6 ± 0.09	3.537 ± 0.0005
0.6	1.5	294	9.16	24.3 ± 0.02%	16.2 ± 0.01%	74.7 ± 0.08	3.513 ± 0.0006
0.6	2	294	12.22	26.7 ± 0.02%	15.2 ± 0.01%	65.8 ± 0.12	3.511 ± 0.0007
0.6	2.5	294	15.27	28.4 ± 0.02%	14.1 ± 0.01%	60.2 ± 0.06	3.303 ± 0.0004
0.7	1	294	7.15	22.1 ± 0.02%	17.3 ± 0.01%	90.6 ± 0.16	3.302 ± 0.0008
0.5	2	294	10.15	25.0 ± 0.02%	14.2 ± 0.01%	68.5 ± 0.13	2.944 ± 0.0005
0.5	1.5	294	7.61	22.5 ± 0.02%	15.0 ± 0.01%	77.1 ± 0.09	2.918 ± 0.0005
0.6	1	294	6.11	20.8 ± 0.02%	16.2 ± 0.01%	90.6 ± 0.05	2.897 ± 0.0004
0.5	2.5	294	12.68	26.7 ± 0.02%	13.3 ± 0.01%	63.0 ± 0.17	2.808 ± 0.0006
0.5	1	294	5.07	18.9 ± 0.02%	14.8 ± 0.01%	91.9 ± 0.05	2.383 ± 0.0003
0.4	2	294	8.07	22.7 ± 0.02%	12.9 ± 0.01%	73.3 ± 0.13	2.270 ± 0.0003
0.4	2.5	294	10.09	24.5 ± 0.02%	13.6 ± 0.01%	81.7 ± 0.09	2.264 ± 0.0003
0.4	1.5	294	6.06	20.2 ± 0.02%	13.5 ± 0.01%	81.7 ± 0.09	2.231 ± 0.0003
0.4	1	294	4.04	16.7 ± 0.01%	13.1 ± 0.01%	95.3 ± 0.05	1.801 ± 0.0002

The results are not surprising when considering the aforementioned two step reaction process. The consideration of the reaction products requirement to escape the capture material to enter the gas in order to deposit energy to generate a signal explains the reason that the system with the most ^{10}B that will operate with the highest FOM.

All of the simulations for 4 mm diameter straws with varying lining thickness surpassed the 1.47 FOM from the ^{10}B-lined tube simulation. Despite this initial success compared to the simple swap out of GERS ^{3}He tubes for GERS ^{10}B-lined tubes, the highest FOM in this set of simulations is only 12.4% of the 18.291 FOM in the original system. The lining thickness in the 4 mm diameter straw simulations is shown in Table 5.1 to be 2 μm thick.

The next set of simulations run have the same variance in lining thickness in 5 mm diameter straws to give more insight of which lining thickness will be optimal and if there is further increase in FOM. The 5 mm diameter straw simulations all surpassed the improved FOM from the ^{10}B-lined simulation and the 4 mm diameter straw simulations. This upward trend shows promise that the increase in diameter will continue to produce a higher FOM, as there will be more neutron capture material. The comparison between the simulations with varying diameter but same thickness will have increasing opportunities for capture reactions while maintaining the same difficulty of the reaction products to escape the liner to enter the proportional gas. Of the four simulations run with 5 mm diameter straws, 2 μm thick lining is shown to have the highest FOM in Table 5.1. Even with this increase in FOM, the rate of increase indicates doubt that the standard footprint of the AWCC will be able to match the original system with BCS.

The next set of simulations were conducted with 6 mm diameter straws with the same lining thickness as the preceding simulations. The FOM has continued to increase as the trend from the 4 mm diameter straws to 5 mm diameter straws suggested. The rate at which the FOM has increased was less than that from 4 mm to 5 mm diameter straws, which further points to the initial conclusion that reaching the FOM of the AWCC with ^{3}He seems unfeasible. For the set of 6 mm diameter straw simulations, the 1.5 μm thick lining straws result in the highest FOM. The

following sets of simulations with diameter increase indicate that this is an inflection point where the optimal thickness changes relative to the diameter of the straws. This result suggests that an increase in diameter of the straws increases neutron capture sites, but also decreases the probability that the reaction products can enter the gas to deposit sufficient energy for a signal.

The next set of simulations for analysis provide more evidence on whether or not the system with BCS in the same HDPE footprint reaches an acceptable FOM for operation. The 7 mm diameter straw simulations show that the increase in diameter of the straws has continued to increase the FOM of the system. Similar to the set of 6 mm diameter straws simulations, the 7 mm diameter set also results in an optimal lining thickness of 1.5 μm. This diameter increase resulted in a greater difference between the FOM from the 1.5 μm and 2 μm simulations, which further suggests that the hypothesis that the 6 mm set of simulations is an infection point for optimal lining thickness is true. The final set of simulations with a diameter increase further supports this theory.

There is not enough room for a full 1 mm increase in straw diameter for the final set of simulations, so 7.8 mm straws are implemented in the final set for analysis with the same variation in lining thickness. The 7.8 mm diameter straw simulations showed further increase in FOM, albeit the smallest increase in FOM from consecutive data sets. This could be because the increase in diameter was 0.2 mm less than that from the previous simulations. The optimal thickness was 1.5 μm in this set of simulations, similar to the 6 mm and 7 mm diameter simulation sets.

The simulation results from the twenty simulations that are composed of the characteristics described above are shown in Figure 5.5. This representation of the data clarifies the preceding analysis of Table 5.1 in graphical representation. Figure 5.5 more clearly indicates

the optimal lining thickness for each of the specified diameter widths used in this research effort. There indistinguishability in the optimal lining thickness for the 6 mm diameter scenario in the figure. In addition to the obviously unique optimal lining thickness for the four other diameter scenarios, this further illustrates the existence of an inflection point when altering the BCS diameter and lining thickness.

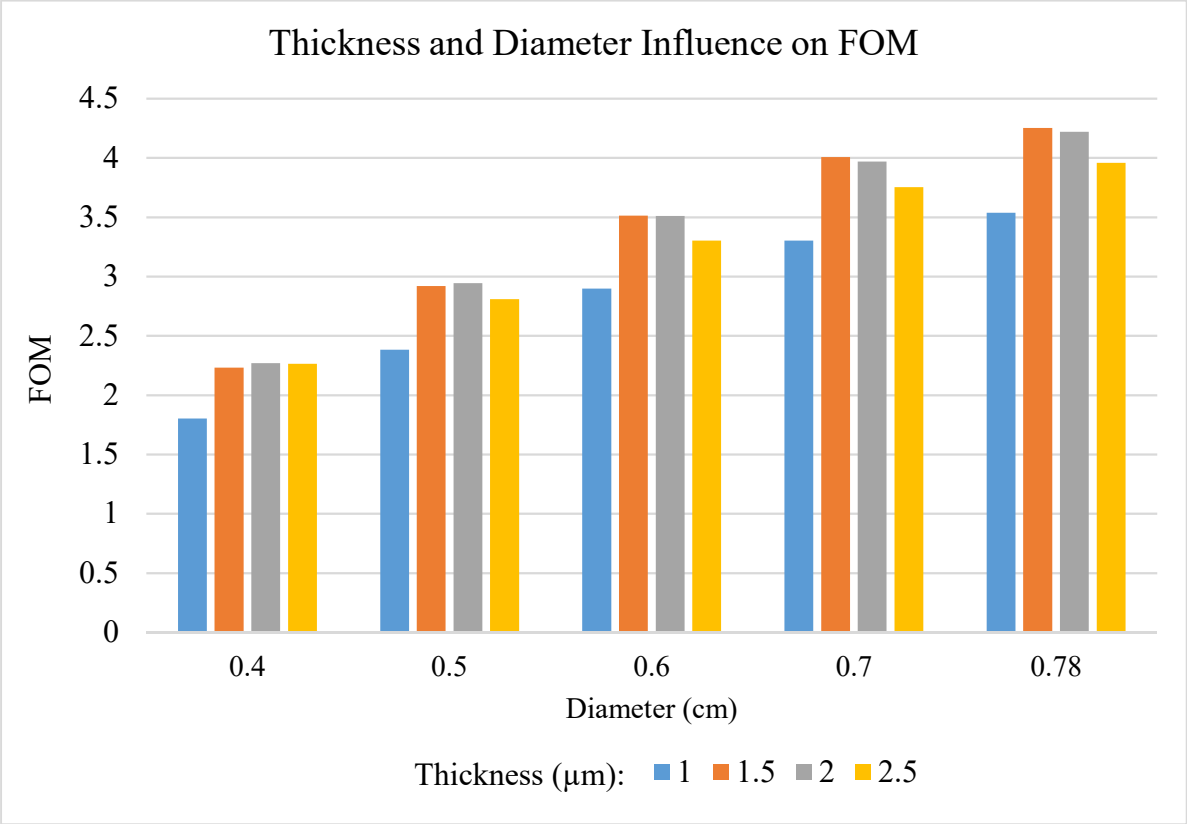

Figure 5.5 Thickness and Diameter Influence on FOM.

An overall trend from all of the simulation sets shown in Table 5.1 is the percentage of captured neutrons which result in a signal generation. Regardless of diameter size, all simulations with 1 µm thick lining show that roughly 78% of neutrons captured deposit enough

energy to elicit a signal. Each increase in lining thickness results in a decrease of the number of captured neutrons which will eventually register a count. All simulations with 1.5 μm thick lining result in approximately 66% of captured neutrons producing a signal. Simulations with 2 μm and 2.5 μm of lining in the BCS shows roughly 57% and 50% of neutron captures cause a signal, respectively.

Another general observation of the entire data set is that the τ decreases as the lining thickness increases. The ten simulations that result in the fastest τ in Table 5.1 all BCS come from models with a lining thickness of 2 μm or 2.5 μm. This is a predictable outcome; the less neutron capture material there is, the longer it will take for a neutron to be captured from the time it is born.

The best FOM from all simulations came from the model with 7.8 mm diameter straws that had 1.5 μm thick lining. This simulation with a FOM of 4.253 is still not an acceptable replacement for the original system, so additional straws will be added to two more simulations in an attempt to further increase the FOM.

5.3 Additional Boron-Coated Straws

As can be seen in the cross-section of the individual tubes which contain the BCS in Figure 5.4, there is enough room to fit more straws in the configurations that utilize 4 mm or 5 mm straws. A decrease in the size of each individual cell in the hexagonal lattice allowed for implementing six more straws than in the original models. By adding these six additional straws, the moderating material within the tubes are reduced by the space of the newly added tubes. In an attempt to further increase the surface area and neutron capture sites, simulations were run

with thirteen BCS with each of the two possible straw diameters. The cross section of 4 mm diameter straws in a bundle of thirteen is shown in Figure 5.5.

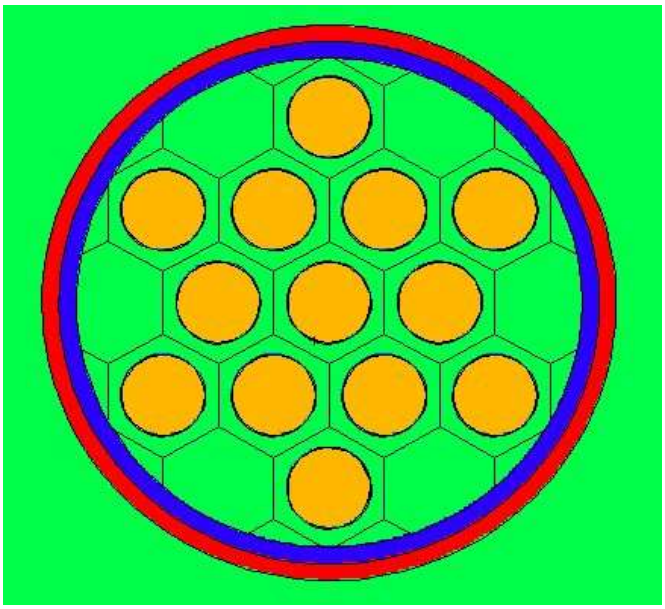

Figure 5.6 GERS Tube with thirteen 4 mm BCS.

The only other straw diameter with sufficient room for more straws is the 5 mm diameter simulation. These two straw diameter simulations are composed of the same geometry with thirteen straws, rather than the original seven straw bundle. This will increase the capture material, but reduce the amount of moderating material. Both of these attributes together are expected to increase the amount of capture reactions while decreasing the τ for a significant increase of FOM from the data discussed in the preceding section.

The two lining thicknesses selected for this final set of simulations was chosen from the preceding section to be 2 μm thick. This lining thickness resulted in the highest FOM for each of the two sets of data and it is assumed will result in the highest FOM for a thirteen straw bundle

as well. This step produces a higher FOM than all of the simulations previously discussed, so future work may be done to alter the HDPE footprint while maintaining the same detection size in an effort to further improve upon the findings of this research. Figure 5.6 shows the cross section of the tube with thirteen 5 mm BCS.

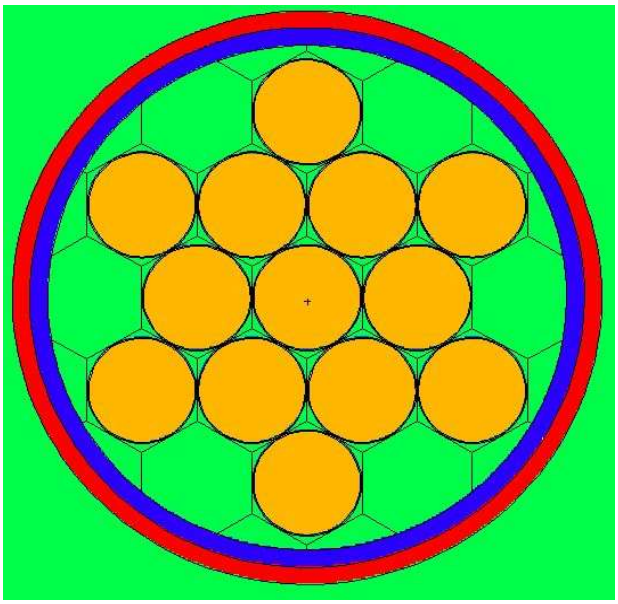

Figure 5.7 GERS Tube with thirteen 5 mm BCS.

The results of the two simulations with thirteen BCS are shown in Table 5.2. Including the six additional straws increased the FOM for each of the two sets of data for each respective straw diameter. Figure 5.6 gives the illusion that the outer tube diameter has increased in size, but this is not in fact the case. The outer aluminum casing is of the same diameter as all of the other simulations.

Table 5.2 Results from AWCC with 13 BCS per tube.

Diameter (cm)	Thickness (μm)	# Straws	^{10}B (g)	Total Captured	TCE	τ (μsec)	FOM
0.5	2	546	18.84	28.8 ± 0.02%	16.4 ± 0.01%	58.1 ± 0.2	4.629 ± 0.002
0.4	2	546	14.99	27.8 ± 0.06%	15.9 ± 0.04%	60.4 ± 0.2	4.186 ± 0.001

The simulation that implemented thirteen BCS of 5 mm diameter and 2 μm thick ^{10}B-lining resulted in the highest FOM of this research. This FOM is only 25.3% of the FOM as the original AWCC with ^{3}He as the detection and signal generating material. More complex geometries could be used to further increase the FOM with BCS, but an increase of quadruple the FOM seems unfeasible within the original footprint of the HDPE in the AWCC. Future exploration will need to incorporate more tubes in an effort to close the gap between the FOM of the original system with BCS.

The configuration with thirteen 4 mm diameter and 2 μm thick ^{10}B-lining resulted in the fourth highest FOM and had only the seventh most amount of ^{10}B. This result suggests that as the number of straws (resulting in higher surface area) seems to be a more important characteristic in producing a detection system with a higher FOM than simply the amount of detection material. This is a useful observation for future work to develop a system with a closer FOM to the original AWCC with ^{3}He gas.

6. CONCLUSIONS

The models developed in search of an acceptable replacement for ^{3}He for an AWCC were compared to the model of the AWCC with ^{3}He as a baseline. The AWCC models developed with ^{10}B were simulated as a starting point to give a rough estimate of how many BCS would be needed to reach the same efficiency as the ^{3}He system.

Various configurations were modeled with the BCS in an attempt to increase the TCE and reduce the τ. The first model that utilized ^{10}B as the detection medium indicated that a replacement technology would require many more tubes. It was calculated that an AWCC requires 69 more ^{10}B-lined tubes to have the same number of capture reactions as the original system. This is unfeasible and would greatly increase footprint of this particular well detector.

In an attempt to increase the number of capture reactions, seven BCS were put into the tubes to increase the area of the surface lining in the MCNPX simulations. The thickness was then manipulated in various simulations in an effort to mitigate wall effects and increase the TCE while simultaneously decreasing the τ.

Table 6.1 is a consolidation of results from all of the simulations that were run in this research effort. The table is sorted from largest to smallest FOM. An AWCC with ^{3}He is still the gold-standard of detection medium when used in the original footprint. The ^{10}B-lined tube simulation resulted in the lowest FOM of this research endeavor. All of the 24 simulations run with BCS successfully surpassed the FOM of the ^{10}B-lined neutron detection system, as predicted.

In general, as the mass of ^{10}B increased in the simulations, so did the total percentage of neutrons captured. This did not translate to an increased FOM, however, due to the lower percentage of the reaction products that were able to enter the proportional gas to deposit enough

energy to elicit a signal. The original system with ^{3}He as the neutron capture and signal generating medium had the same Total Captured percentage as TCE, as expected. Simulations with 1 μm thick lining in a BCS system resulted in approximately 78% of the neutrons captured depositing enough energy to register a count, regardless of the straw diameter. As the lining thickness increased, the percentage of neutrons captured decreased. Simulations with a lining that is 1.5 μm thick in the BCS showed roughly 66% of the neutrons captured result in a count. Each simulation with 2 μm and 2.5 μm of lining in the BCS shows approximately 57% and 50% of the captured neutrons causing a signal, respectively.

Despite the lower percentage of reaction products that enter the gas in the thicker linings, the five configurations that operate with a FOM over 4 are either 1.5 or 2 μm thick. This outcome suggests that the optimal range for the lining in BCS is between 1.5 and 2 μm. When the lining thickness is either 1.5 μm or 2 μm, the increase in neutron capture material compensates for the lower percentage of reaction products able to enter the gas. This is done while simultaneously not being too thick to have a diminishing effect on the counts registered.

The increased τ contributed to the lower FOM of the BCS simulations that had 1 μm lining. This is to be expected; as there is less neutron capture material, it will take longer for a neutron to be absorbed from the time of its birth. Shortest τ is correlated with the amount of neutron capture material, which is shown by the ten simulations with the fastest τ all having BCS with either 2 or 2.5 μm thick lining.

In the balance between increasing TCE and decreasing τ, the simulation with 13 straws per tube for a total of 546 straws with 2 μm thick lining operates with the highest FOM. This simulation had the second highest mass of ^{10}B. The increase in neutron capture material combined with the increase in surface area results in a model with the third most captures, fifth

highest TCE, and third fastest τ. Despite not having the highest value in the contributing categories to FOM, the combination of high TCE and fast τ produce the highest FOM of the simulations that were run.

The improvement from the baseline model with ^{10}B-lined tubes to the model with 546 BCS that have 2 μm lining was a 315% increase in FOM. In order to match the original ^{3}He AWCC, the highest performing simulation with BCS would need to increase FOM by 395%. With the constraint of using the same footprint as the original system, this was unfeasible. The results of this study show promise in an acceptable replacement if the footprint can be manipulated. An increase in the number of tubes that contain 13 BCS that have 2 μm thick lining could improve the FOM further. The scope of this work was to find the optimal system that utilized BCS, which was successful. Future work and investigation into the cost of manipulating the footprint of the detector could make this new technology an attractive replacement.

Table 6.1 Compilation of results from all simulations (the green cells utilize 42 detectors, orange cells have 546, and the remainder have 294).

Medium	Diam. (cm)	Press. (atm)	Thick (μm)	Mass (g)	Total Captured	TCE	τ (μsec)	FOM
^{3}He	2.54	4	N/A	8.9	30.9 ± 0.02%	30.9 ± 0.02%	52.2 ± 0.02	18.291 ± 0.007
BCS	0.5	0.7	2	18.84	28.8 ± 0.02%	16.4 ± 0.01%	58.1 ± 0.19	4.629 ± 0.002
	0.78	0.7	1.5	11.96	26.3 ± 0.02%	17.5 ± 0.01%	72.0 ± 0.05	4.253 ± 0.001
	0.78	0.7	2	15.95	28.5 ± 0.02%	16.2 ± 0.01%	62.2 ± 0.08	4.219 ± 0.001
	0.4	0.7	2	14.99	27.8 ± 0.02%	15.9 ± 0.01%	60.4 ± 0.23	4.186 ± 0.001
	0.7	0.7	1.5	10.72	25.6 ± 0.02%	17.1 ± 0.01%	73.0 ± 0.07	4.006 ± 0.001
	0.7	0.7	2	14.29	27.9 ± 0.02%	15.9 ± 0.01%	63.7 ± 0.11	3.969 ± 0.001
	0.78	0.7	2.5	19.93	30 ± 0.02%	14.9 ± 0.01%	56.1 ± 0.11	3.957 ± 0.001
	0.7	0.7	2.5	17.86	29.5 ± 0.02%	14.7 ± 0.01%	57.6 ± 0.14	3.752 ± 0.001
	0.78	0.7	1	7.97	22.9 ± 0.02%	17.9 ± 0.01%	90.6 ± 0.09	3.537 ± 0.001
	0.6	0.7	1.5	9.16	24.3 ± 0.02%	16.2 ± 0.01%	74.7 ± 0.08	3.513 ± 0.001
	0.6	0.7	2	12.22	26.7 ± 0.02%	15.2 ± 0.01%	65.8 ± 0.12	3.511 ± 0.001
	0.7	0.7	1	7.15	22.1 ± 0.02%	17.3 ± 0.01%	90.6 ± 0.06	3.303 ± 0.000
	0.6	0.7	2.5	15.27	28.4 ± 0.02%	14.1 ± 0.01%	60.2 ± 0.16	3.302 ± 0.001
	0.5	0.7	2	10.15	25 ± 0.02%	14.2 ± 0.01%	68.5 ± 0.13	2.944 ± 0.001
	0.5	0.7	1.5	7.61	22.5 ± 0.02%	15.0 ± 0.01%	77.1 ± 0.09	2.918 ± 0.000
	0.6	0.7	1	6.11	20.8 ± 0.02%	16.2 ± 0.01%	90.6 ± 0.05	2.897 ± 0.000
	0.5	0.7	2.5	12.68	26.7 ± 0.02%	13.3 ± 0.01%	63.0 ± 0.17	2.808 ± 0.001
	0.5	0.7	1	5.07	18.9 ± 0.02%	14.8 ± 0.01%	91.9 ± 0.05	2.382 ± 0.000
	0.4	0.7	2	8.07	22.7 ± 0.02%	12.9 ± 0.01%	73.3 ± 0.13	2.270 ± 0.000
	0.4	0.7	2.5	10.09	24.5 ± 0.02%	13.6 ± 0.01%	81.7 ± 0.09	2.264 ± 0.000
	0.4	0.7	1.5	6.06	20.2 ± 0.02%	13.5 ± 0.01%	81.7 ± 0.09	2.231 ± 0.000
	0.4	0.7	1	4.04	16.7 ± 0.01%	13.1 ± 0.01%	95.3 ± 0.05	1.801 ± 0.000
^{10}B-Lined	2.54	0.7	2.5	10.15	24 ± 0.02%	11.7 ± 0.01%	93.3 ± 0.07	1.467 ± 0.000

REFERENCES

[1] Joy, DR. An Introduction to The Nuclear Fuel Cycle and Nuclear Safeguards. JAI Corporation. Fairfax, Virginia. October 1999.

[2] The Statute of the IAEA. (2014, June 02). Retrieved September 12, 2017, from https://www.iaea.org/about/statute#a1-2.

[3] Treaty on the Non-Proliferation of Nuclear Weapons (NPT). May 11, 1995. Retrieved September 12, 2017, from https://www.un.org/disarmament/wmd/nuclear/npt/.

[4] Menlove, HO. Description and Operation Manual for the Active Well Coincidence Counter. Los Alamos National Laboratory. LA-7823-M. May 1979.

[5] Canberra Industries, Inc. Model JCC-51 Active Well Coincidence Counter. May 2009.

[6] Ensslin, N. Principles of Neutron Coincidence Counting. Passive Nondestructive Assay Manual (PANDA). Los Alamos National Laboratory. LA-UR-90-732. March 1991.

[7] Steidl, M. KIT - KATRIN -Measurement principle. Retrieved from: https://www.katrin.kit.edu/79.php

[8] Kayani, SA. US and Russia's Determination towards Global Zero. December 29, 2014. Retrieved from: http://foreignpolicynews.org/2014/12/29/us-russias-determination-towards-global-zero/

[9] Slocum, CA. Defining Helium-3 Industry for Private Sector. Arizona Oil and Gas Inc. August 1, 2016.

[10] Shea, DA; Morgan, D. The Helium-3 Shortage: Supply, Demand, and Option for Congress. Congressional Research Service. R-41419. December 22, 2010.

[11] Tyler, C. Running Low. Los Alamos Science and Technology Magazine. Los Alamos National Laboratory. August 2014.

[12] Crane, TW; Baker, MP. Neutron Detectors. Passive Nondestructive Assay Manual (PANDA). Los Alamos National Laboratory. LA-UR-90-732. March 1991.

[13] Ely, JH; Siciliano, ER; Swinhoe, MT; Lintereur, AT. Modeling and Simulation Optimization and Feasibility Studies for the Neutron Detection without Helium-3 Project, Pacific Northwest National Laboratory, Pacific Northwest National Laboratory PNNL-22228 (2013).

[14] X-5 Monte Carlo Team, MCNP – A General Monte Carlo N-Particle Transport Code, Version 5, Los Alamos National Laboratory LA-UR-03-1987 (2003).

[15] Pelowitz, DB; Durkee, JW; Elson, JS; Fensin, ML; Hendircks, JS; James, MR; Johns, RC; McKinney, GW; Mashnik, SG; Verbecke, JM; Waters, LS; Wilcox, TA. MCNPX 2.7.0 Extensions, Los Alamos National Laboratory LA-UR-11-02295 (2011).

[16] "FICHIER model51," MCNP model of the JCC-51 by Anne-Laure Weber, CEA/IPSN/DSMR/SATE, Commissariat L'Energie Atomique (CEA) European Safeguards Research & Development.

[17] Amaro, FD; Monteiro, CMB; Dos Santos, JMF; Antognini, A. Novel concept for neutron detection: proportional counter filled with ^{10}B nanoparticle aerosol. Scientific Reports. PMID: 28181520. February 9, 2017.

[18] McElroy, RD; Croft, S. Application of ^{10}B-Lined Proportional Counters to Traditional Neutron Counting Applications in International Safeguards. Oak Ridge National Laboratory. 2014.

[19] Lacy, JL. Boron Coated Straw Neutron Detector. Proportional Technologies, Inc., assignee. Patent WO2004043372A2. May 11, 2003. Print.

[20] Technology. Proportional Technologies, Inc. Retrieved from: https://proportionaltech.myshopify.com/pages/technology

[21] Lacy, JL; Athanasiades, A; Sun, L; Martin, CS; Lyons, TD; Foss, MA; Haygood, HB. Boron-Coated Straws as a Replacement for ^{3}He-Based Neutron Detectors. Nuclear Instruments and Methods in Physics Research Section A: Accelerators, Spectrometers, Detectors and Associated Equipment. October 2011.

[22] Kouzes, RT; Siciliano, ER. Boron-10 Lined Proportional Counter Wall Effects. Pacific Northwest National Laboratory. PNNL-21368. May 2012.

[23] Lacy, JL; Athanasiades, A; Sun, L; Martin, CS; Vazquez-Flores, GJ. Boron Coated Straw Detectors as a Replacement for ^{3}He. Nuclear Science Symposium Conference Record (NSS/MIC), 2009 IEEE. October 24 – November 1, 2009.